

VGAS: Value-Guided Action-Chunk Selection for Few-Shot Vision-Language-Action Adaptation

Changhua Xu, Jie Lu, Junyu Xuan, En Yu

Australian Artificial Intelligence Institute (AAII), University of Technology Sydney, Australia
 changhua.xu@student.uts.edu.au; {jie.lu, junyu.xuan, en.yu-1}@uts.edu.au

Abstract

Vision-Language-Action (VLA) models bridge multimodal reasoning with physical control, but adapting them to new tasks with scarce demonstrations remains unreliable. While fine-tuned VLA policies often produce semantically plausible trajectories, failures often arise from unresolved geometric ambiguities, where near-miss action candidates lead to divergent execution outcomes under limited supervision. We study few-shot VLA adaptation from a *generation-selection* perspective and propose a novel framework **VGAS** (Value-Guided Action-chunk Selection). It performs inference-time best-of- N selection to identify action chunks that are both semantically faithful and geometrically precise. Specifically, **VGAS** employs a fine-tuned VLA as a high-recall proposal generator and introduces the Q-Chunk-Former, a geometrically grounded Transformer critic to resolve fine-grained geometric ambiguities. In addition, we propose *Explicit Geometric Regularization* (EGR), which explicitly shapes a discriminative value landscape to preserve action ranking resolution among near-miss candidates while mitigating value instability under scarce supervision. Experiments and theoretical analysis demonstrate that **VGAS** consistently improves success rates and robustness under limited demonstrations and distribution shifts. Our code is available at <https://github.com/Jyugo-15/VGAS>.

1 Introduction

Vision-Language-Action (VLA) models have emerged as a transformative paradigm for embodied AI, bridging multimodal reasoning with physical control [Brohan *et al.*, 2022; Zitkovich *et al.*, 2023]. By pretraining on vast robotic datasets, these generalist policies learn to map complex visual observations and linguistic instructions directly into executable actions [Black *et al.*, 2024; Kim *et al.*, 2024; Team *et al.*, 2024]. However, the reliability of VLAs in downstream applications remains heavily bottlenecked by the prevailing Supervised Fine-Tuning (SFT) paradigm [Kim *et al.*, 2025; Zhang *et al.*, 2025]. SFT-based adaptation demands a high

volume of expert demonstrations to bridge the gap between generalist priors and task-specific requirements. This is often challenging in real-world environments where high-quality robotic data collection is costly, unscalable, and prone to out-of-distribution (OOD) uncertainties [Dass *et al.*, 2022; Xin *et al.*, 2024; Sapkota *et al.*, 2025]. Consequently, under data-scarce regimes, VLA policies often exhibit brittle performance, failing to generalize across even minor distribution shifts [Liu *et al.*, 2025; Li *et al.*, 2025a; Yu *et al.*, 2025].

To concretely examine this data-scarce regime, we simulate a few-shot adaptation setting that reflects realistic deployment constraints. Specifically, we fine-tune a pretrained VLA policy with five task demonstrations and evaluate its execution behavior on novel task instances. As shown in Figure 1, a fine-tuned VLA often produces semantically plausible actions (e.g., reaching the correct object) around the ground-truth actions (shown in red), yet fails at execution due to subtle geometric errors such as imprecise grasps or joint-angle overshoot [Kumar *et al.*, 2022]. These near-miss candidates often reside in the high-likelihood regions of the policy’s output distribution, making them indistinguishable through standard likelihood-based SFT objectives. This suggests that a primary bottleneck in few-shot VLA adaptation is geometric rather than semantic. We therefore recast adaptation as a value-guided selection problem: instead of forcing a generative policy to jointly learn semantics and precise geometric control end-to-end under sparse supervision, we decouple high-recall proposal generation from a high-precision selection stage that favors candidates with the highest chance of long-horizon success.

Offline Reinforcement Learning (ORL) provides a natural framework for this selection objective, as it learns an

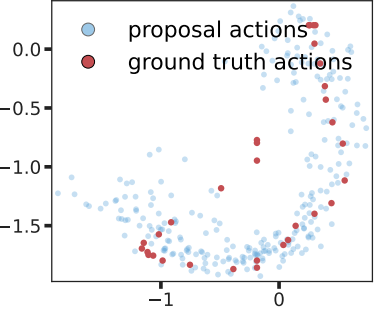


Figure 1: Illustration of near-miss actions distribution under 5-shot VLA fine-tuning.

outcome-aware critic that maps long-horizon success into a scalar value signal [Sutton *et al.*, 1998]—perfectly suited for ranking candidate proposals [Ghasemipour *et al.*, 2021]. However, applying existing ORL methodologies to modern VLA policies exposes two fundamental limitations: 1) *Structural and observational mismatch*: Standard RL assumes per-step atomic actions, whereas modern VLAs output temporally extended action chunks, inducing an SMDP structure that complicates value learning and temporal credit assignment [Sutton *et al.*, 1999]. Moreover, most offline RL is evaluated with compact, near-Markovian state inputs; in contrast, VLA relies on high-dimensional vision-language observations with geometric grounding, making value estimation substantially harder and comparatively under-explored [Fu *et al.*, 2020; Lu *et al.*, 2022]. 2) *Ranking resolution vs. conservatism*: Offline RL often controls extrapolation under distribution shift via conservative objectives or behavior-regularized extraction [Kumar *et al.*, 2020; Kostrikov *et al.*, 2021]. In few-shot sparse-reward settings, however, such regularization can compress value gaps among proposal-supported “near-miss” candidates, yielding low-contrast gradients and weakening inference-time Best-of- N selection [Lyu *et al.*, 2022]. These limitations raise two major research questions: **RQ1**. *What critic architecture can robustly ground high-dimensional VLA observations into precise value estimates for temporally extended action chunks?* and **RQ2**. *How can a value function be trained on demonstration-heavy data to maintain high ranking resolution under scarce supervision and distribution shifts?*

To address these questions, we propose **VGAS** (Value-Guided Action-chunk Selection) for VLA adaptation via generation–selection decoupling. For **RQ1**, we introduce Q-Chunk-Former, a geometrically grounded critic architecture built on a Transformer backbone. By leveraging the Transformer’s sequence modeling capability, our design naturally captures temporal dependencies within action chunks. Crucially, our architecture preserves fine-grained, token-level features, allowing attention to explicitly focus on geometric cues that are critical for precise value estimation. For **RQ2**, we propose a hybrid offline RL objective that *anchors* temporal consistency via a proposal-constrained Bellman backup, augmented by Explicit Geometric Regularization (EGR). Unlike traditional conservative methods that indiscriminately penalize out-of-distribution actions, EGR injects dense geometric supervision, shaping the value landscape into a smooth funnel anchored at expert demonstrations. This allows the critic to maintain high ranking resolution among “near-miss” candidates even under scarce supervision. Our contributions are summarized as follows:

- We reformulate few-shot VLA adaptation as a value-guided selection problem and propose the novel **VGAS** method, shifting the paradigm from likelihood-based generation to outcome-aware ranking.
- We propose Q-Chunk-Former, which enables precise geometric grounding for action-chunk evaluation. We introduce EGR, a regularization technique that injects dense geometric priors into offline RL to maintain high ranking resolution under data-scarce regimes.

- We provide theoretical guarantees for the convergence of our chunk-level value operator and demonstrate through extensive experiments on the LIBERO benchmark that VGAS consistently outperforms SFT and standard ORL baselines, particularly in terms of success rate and robustness under distribution shifts.

2 Preliminary

Offline Reinforcement Learning We consider a Markov Decision Process (MDP) defined by $\mathcal{M} = (\mathcal{S}, \mathcal{A}, \mathcal{P}, r, \rho, \gamma)$, where $s \in \mathcal{S}$, $a \in \mathcal{A}$, $\mathcal{P}(s' \mid s, a)$ is the transition kernel, $r(s, a) \in \mathbb{R}$ is the reward function, $\rho \in \Delta(\mathcal{S})$ is the initial-state distribution, and $\gamma \in [0, 1)$ is the discount factor. The objective is to learn a policy π maximizing the expected discounted return $J(\pi) = \mathbb{E}_\pi \left[\sum_{t \geq 0} \gamma^t r(s_t, a_t) \right]$.

Value-based methods estimate the optimal action-value function Q^* as the fixed point of the Bellman optimality operator:

$$(\mathcal{T}^* Q)(s, a) = r(s, a) + \gamma \mathbb{E}_{s' \sim \mathcal{P}(\cdot \mid s, a)} \left[\max_{a' \in \mathcal{A}} Q(s', a') \right]. \quad (1)$$

In offline RL, the agent learns from a fixed dataset \mathcal{D} collected by a behavior policy π_β , without additional environment interaction. A key challenge is extrapolation error: the maximization over a' may select actions outside the data support, leading to overestimation and instability. Many offline RL methods [Shin and Kim, 2023] mitigate this via conservative regularization [Kumar *et al.*, 2020], which discourages high values on out-of-distribution actions.

Action Chunking in VLAs Modern VLAs condition on multimodal inputs, which we denote by the state $s_t = (I_t, L_t, p_t)$, comprising visual tokens I_t , language instruction L_t , and robot proprioception p_t [Zitkovich *et al.*, 2023; Brohan *et al.*, 2022]. With a slight abuse of notation, we treat this policy input as the MDP state. Instead of per-step control, these models often output a temporally extended *action chunk* with horizon h :

$$A_t := (a_t, \dots, a_{t+h-1}) \in \mathcal{A}^h, \quad A_t \sim \pi_\mu(\cdot \mid s_t). \quad (2)$$

Few-shot VLA adaptation objective. Given a few-shot expert dataset $\mathcal{D} = \{\tau_i\}_{i=1}^K$, we first obtain a task-aligned base chunk policy $\pi_\mu(A \mid s)$ (e.g., via SFT on \mathcal{D}). In few-shot regimes, such SFT is typically semantically correct but geometrically imprecise: it captures the demonstrated mode yet struggles to resolve fine-grained geometric ambiguities. We therefore treat π_μ as a high-recall proposal distribution and assume it retains non-trivial *local recall* around each demonstrated chunk,

$$\pi_\mu(\{A : \|A - A_t\|_2 \leq \varepsilon\} \mid s_t) \geq p_0, \forall (s_t, A_t) \in \mathcal{D}, \quad (3)$$

for some $\varepsilon > 0$ and $p_0 > 0$. Intuitively, p_0 ensures the proposal covers valid near-miss candidates. Our goal is to improve upon π_μ by learning an offline-adapted chunk policy within a proposal-constrained class Π_μ :

$$\pi^* := \arg \max_{\pi \in \Pi_\mu} J(\pi), \quad (4)$$

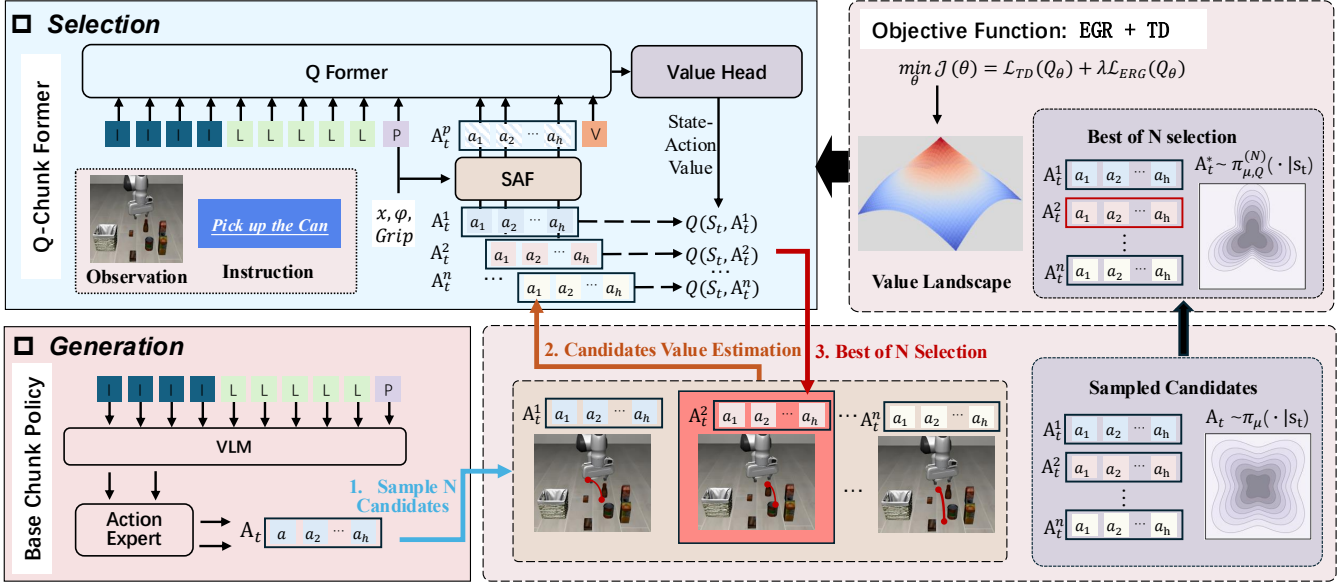


Figure 2: The overall framework of VGAS. **Generation:** A fine-tuned VLA policy proposes N candidate action chunks from multimodal inputs. **Selection:** Q-Chunk-Former learns a scoring function Q via the EGR+TD objective. Best-of- N selection defines the induced policy $\pi_{\mu,Q}^{(N)}$ by maximizing over a discriminative value landscape shaped by EGR, prioritizing expert-aligned candidates and thereby mitigating geometric drift.

where Π_μ denotes policies supported by (or centered at) the proposal π_μ . Under chunked execution, the return is

$$J(\pi) := \mathbb{E}_{\tau \sim \pi} \left[\sum_{k=0}^{\infty} (\gamma^k)^k R_h(s_{t_k}, A_{t_k}) \right] \quad (5)$$

where $t_k = kh$ denotes the start time of the k -th chunk, $A_{t_k} \sim \pi(\cdot | s_{t_k})$ is the action chunk, and $R_h(s_{t_k}, A_{t_k}) = \sum_{j=0}^{h-1} \gamma^j r(s_{t_k+j}, a_{t_k+j})$ is the discounted cumulative reward over the chunk.

3 Methodology

Framework Overview. VGAS reformulates few-shot VLA adaptation as a generate-then-select process. As illustrated in Figure 2, our pipeline decouples the policy into two components: a *high-recall generator* and a *high-precision critic*. First, we utilize a supervised fine-tuned (SFT) VLA model as the base policy $\pi_\mu(A_t | s_t)$ to provide a proposal distribution covering plausible action chunks. At inference time, we sample N candidates $\{A_t^{(i)}\}_{i=1}^N \sim \pi_\mu(\cdot | s_t)$ and employ a learned critic Q_θ to execute Best-of- N selection, $A_t^* = \arg \max_i Q_\theta(s_t, A_t^{(i)})$. This strategy approximates policy improvement within the support of π_μ , prioritizing geometric precision without requiring online exploration.

To realize this selection mechanism effectively, VGAS addresses two core challenges: *representation* and *optimization*. First, regarding critic representation (Sec.3.1), we introduce Q-Chunk-Former, a Transformer-based architecture tailored for VLA inputs. To prevent high-dimensional visual tokens from overwhelming physical cues, we design a State-Action Fusion (SAF) module that explicitly grounds action chunks in

proprioceptive states before multimodal integration. Second, for critic optimization (Sec.3.2), we propose a hybrid learning objective that combines temporal and spatial supervision. We stabilize offline training using a *Proposal-Constrained Chunked Expected-Max* backup, which enforces temporal consistency across action chunks. We further augment this with *Explicit Geometric Regularization* EGR, a dense supervision signal that directly shapes the value landscape based on geometric proximity to expert demonstrations, enabling the critic to reliably distinguish near-miss actions from failures even under sparse task rewards.

3.1 Q-Chunk-Former

To optimize the few-shot adaptation objective in Eq. (4), the critic network must accurately estimate the long-horizon value of a temporally extended action chunk A_t given state s_t . This imposes two key requirements. (i) Chunk-level evaluation with temporal structure: the critic must assign a single long-horizon value to an entire action chunk A_t for Best-of- N selection (Eq. 9), while preserving the within-chunk temporal ordering of actions. (ii) Multimodal fusion without geometric collapse: unlike classical critics operating on compact state vectors, VLA conditioning involves heterogeneous inputs such as vision, language, and proprioception, where naive compression can discard geometry-critical cues needed for feasibility-aware value estimation.

Motivated by token-level multimodal modeling [Marafioti *et al.*, 2025], we introduce a Transformer-based critic. A naive design treats all modalities as a single concatenated token sequence:

$$Q_\theta(s_t, A_t) = \text{Transformer}_\theta([I_t, L_t, p_t, A_t]), \quad (6)$$

where $[\cdot]$ denotes concatenation. However, in practice, the self-attention mechanism tends to be dominated by the abundant visual and linguistic tokens, so the single proprioceptive token p_t receives insufficient attention. This is detrimental because value estimation for manipulation requires joint reasoning over the external world context (from I_t and L_t) and the internal robot state (embodiment and configuration encoded by p_t). If p_t is under-utilized, the critic becomes less sensitive to geometric feasibility, weakening feasibility-aware value estimation.

To address this, we introduce a lightweight State-Action Fusion (SAF) module that conditions the raw chunk A_t on p_t prior to mixing with high-dimensional perceptions. The SAF module produces proprioception-grounded action tokens A_t^p ,

$$A_t^p = \text{SAF}(A_t, p_t) = W_{\text{fuse}}([W_a A_t \| W_p p_t]), \quad (7)$$

where W_a and W_p are learnable projections mapping inputs to a shared latent space and W_{fuse} aggregates the concatenated features. This design enforces a high-fidelity interaction between action tokens and the proprioceptive state, ensuring that feasibility cues are embedded directly into the chunk representation.

The grounded action tokens A_t^p are then integrated with the frozen perceptual tokens¹ and a learnable [VALUE] token v via a Transformer decoder, denoted as the Q-Former (QF). Finally, a Value Head (VH) maps the output embedding of v to a scalar Q-value:

$$Q_\theta(s_t, A_t) = \text{VH}(\text{QF}(I_t, L_t, p_t, A_t^p, v)). \quad (8)$$

In summary, Q-Chunk-Former comprises SAF, QF, and VH modules. This architecture mitigates attention imbalance and ensures that value estimation is strictly grounded in geometric reality, providing a reliable signal for selection.

3.2 Optimization Objective

Our goal is to learn a critic that supports *value-guided selection* over a fixed proposal distribution. We assume access to a task-adapted base chunk policy $\pi_\mu(A \mid s)$ that generates semantically plausible action chunks. At inference time, we draw N i.i.d. candidates from π_μ and select the best one according to a scoring rule Q :

$$A_Q^*(s) := \arg \max_{i \in [N]} Q(s, A^{(i)}). \quad (9)$$

Although the maximization in Eq. (9) is deterministic conditioned on the sampled set, proposal sampling induces a stochastic *selection policy*. We denote this induced policy by $\pi_{\mu, Q}^{(N)}(A \mid s)$, defined as the distribution of $A_Q^*(s)$.

To learn Q from a fixed offline dataset \mathcal{D} , we train the critic as a proxy for the long-horizon return of the induced policy $\pi_{\mu, Q}^{(N)}$ in the chunk-induced SMDP. A reliable critic in the few-shot, distribution-shifted regime must satisfy two coupled desiderata: (i) **temporal consistency**, i.e., Bellman-style alignment with the expected *max* return under best-of- N

¹Perceptual tokens I_t and L_t are extracted from the pre-trained VLM encoder of the base policy to ensure feature alignment and computational efficiency.

selection over π_μ samples; and (ii) **spatial consistency**, i.e., preserving fine-grained geometric ranking among near-miss proposals. We instantiate these principles with the following hybrid objective:

$$\min_{\theta} \mathcal{J}(\theta) = \mathcal{L}_{\text{TD}}(Q_\theta) + \lambda \mathcal{L}_{\text{EGR}}(Q_\theta). \quad (10)$$

3.2.1 Temporal Consistency

The primary goal of \mathcal{L}_{TD} is to align critic learning with our inference-time execution, i.e., to learn the value function induced by Best-of- N selection, $\pi_{\mu, Q}^{(N)}$. This alignment requires two ingredients. First, since execution commits to a length- h action chunk, the critic must evaluate the return of an entire chunk. We therefore adopt the chunk-level TD formulation from Q-Chunking [Li *et al.*, 2025b] and learn $Q(s_t, A_t)$ that conditions on the full action chunk.

Second, we must ensure that the *Bellman backup* matches the same Best-of- N rule used at inference. To this end, inspired by Expected-Max Q-learning (EMaQ) [Ghasemipour *et al.*, 2021], the key insight of EMaQ is to construct a Bellman backup that replaces the standard expectation under a policy with an expected maximization over a set of sampled proposals. By targeting this maximum, the objective ensures that the critic trained with this operator is guaranteed to converge to the value function of the corresponding Best-of- N selection policy $\pi_{\mu, Q}^{(N)}$. Thus, we define the proposal-constrained *Chunked Expected-Max* backup operator \mathcal{T}_μ^N as

$$(\mathcal{T}_\mu^N Q)(s, A) := R_h(s, A) + \gamma^h \mathbb{E}_{s' \sim \mathcal{P}_h(\cdot \mid s, A)} \left[\mathbb{E}_{A'_{1:N} \stackrel{\text{i.i.d.}}{\sim} \pi_\mu(\cdot \mid s')} \left[\max_{i \in [N]} Q(s', A'_i) \right] \right], \quad (11)$$

where R_h is the discounted cumulative reward over the chunk and \mathcal{P}_h is the h -step transition kernel. The inner maximization corresponds exactly to selecting $A_Q^*(s')$ from Eq. (9), thereby enforcing strict train–test consistency.

This operator formulation offers rigorous theoretical guarantees for offline adaptation, which we summarize below.

Proposition 1 (Chunked Expected–Max in tabular SMDPs). *In the tabular chunk-induced SMDP, assume bounded rewards and $\gamma^h \in (0, 1)$. Then \mathcal{T}_μ^N in Eq. (11) is a γ^h -contraction under $\|\cdot\|_\infty$ and has a unique fixed point Q_μ^N . Let $\pi_\mu^{(N)} := \pi_{\mu, Q_\mu^N}^{(N)}$ be the induced Best-of- N policy. Then $Q_\mu^N = Q_{\mu, Q_\mu^N}^{(N)}$. Monotonicity in N and the $N \rightarrow \infty$ limit are given in Prop. 3 and Thm. 2 (App. B).*

Proposition 1 shows that the proposed backup is well-defined in the tabular induced SMDP and that its unique fixed point corresponds exactly to the value function of the induced Best-of- N selection policy. A detailed proof of these properties in the tabular SMDP setting is provided in Appendix B.

Based on this operator, we instantiate the final temporal-difference loss using a standard target network $Q_{\bar{\theta}}$ for stability:

$$\mathcal{L}_{\text{TD}}(\theta) = \mathbb{E}_{(s_t, A_t, s_{t+h}) \sim \mathcal{D}} \left[(Q_\theta(s_t, A_t) - y_t)^2 \right], \quad (12)$$

where $y_t = R_h(s_t, A_t) + \gamma^h \max_{i \in [N]} Q_{\bar{\theta}}(s_{t+h}, A_{t+h}^i)$.

Here, the proposals $\{\hat{A}_{t+h}^i\}_{i=1}^N$ are sampled from the frozen proposal distribution $\pi_\mu(\cdot | s_{t+h})$ at the next decision state. This loss provides a stable, proposal-constrained temporal anchor for our critic, paving the way for the spatial regularization described next.

3.2.2 Spatial Consistency

While the proposal-constrained TD loss provides a stable temporal anchor, offline critic learning remains vulnerable to extrapolation error, where OOD (off-demo) candidates deviating from the training data distribution receive spuriously high values. Standard conservative methods, such as CQL [Kumar *et al.*, 2020], mitigate this by indiscriminately suppressing values for all low-support actions. However, in the few-shot regime, this uniform penalty is overly aggressive, because it compresses the value dynamic range within the proposal support candidate and reduces the fine-grained ranking resolution needed to distinguish plausible “near-miss” candidates from catastrophic failures. This “value collapse” directly undermines inference-time Best-of- N selection.

To address this, we introduce *Explicit Geometric Regularization (EGR)*. Instead of uniformly suppressing off-demo actions, EGR serves as a structural regularizer. During training, we regularize the critic with off-demo candidates sampled from $\rho(\cdot | s_t)$ (a proposal-centered mixture with simple augmentations). At inference time, Best-of- N selects only among proposal samples from $\pi_\mu(\cdot | s_t)$. Accordingly, EGR targets two desiderata: **(i) TD-Anchored Calibration**: anchor the value scale to the TD target y_t to mitigate overestimation on off-demo candidates; **(ii) Geometric Discriminability**: within the inference-time proposal set, preserve a graded preference for geometric proximity, providing a smooth signal to separate recoverable near-misses from divergence.

We formalize EGR as the following weighted combination of *Anchoring* and *Ranking* losses.

$$\mathcal{L}_{\text{EGR}}(\theta) = \mathcal{L}_{\text{anchor}}(\theta) + \eta \mathcal{L}_{\text{rank}}(\theta), \quad (13)$$

where $\eta \geq 0$ balances the *absolute scale* (Anchoring) and the *local ordering* (Ranking).

a. Geometric Anchoring ($\mathcal{L}_{\text{anchor}}$). For any off-demo action chunk $\hat{A}_t \sim \rho(\cdot | s_t)$, we define

$$\mathcal{Y}(s_t, \hat{A}_t) := \text{sg}(y_t) - \beta \|\hat{A}_t - A_t\|_{\mathcal{W}}^2, \quad (14)$$

where $\text{sg}(\cdot)$ stops gradients and y_t is the TD target from Eq. (12). Crucially, we do not posit Euclidean distance as a global ground-truth metric; rather, we employ this surface as a *structural inductive bias* to shape the value landscape in regions where task supervision is absent. In our setting, we employ a weighted metric $\|\hat{A}_t - A_t\|_{\mathcal{W}}^2$ to prioritize critical kinematic dimensions (e.g., end-effector position) within the normalized control space. This serves as a robust local proxy for geometric proximity: under smooth dynamics, small weighted action deviations tend to induce small short-horizon trajectory deviations. (See Appendix D.3 for details).

To satisfy TD-anchored calibration, we align the critic’s absolute estimates on candidate chunks with the reference surface:

$$\mathcal{L}_{\text{anchor}}(\theta; s_t, A_t) = \mathbb{E}_{\hat{A}_t \sim \rho(\cdot | s_t)} [\ell(Q_\theta(s_t, \hat{A}_t), \mathcal{Y}(s_t, \hat{A}_t))], \quad (15)$$

where $\ell(\cdot, \cdot)$ is the squared error.

b. Geometric Ranking ($\mathcal{L}_{\text{rank}}$). While anchoring constrains the absolute scale, it does not guarantee robust *local* discrimination. To enforce geometric discriminability, we introduce a pairwise ranking loss. For any pair $(\hat{A}_t^i, \hat{A}_t^j) \sim \rho(\cdot | s_t)$, define squared distances to the expert:

$$d_i := \|\hat{A}_t^i - A_t\|_{\mathcal{W}}^2, \quad d_j := \|\hat{A}_t^j - A_t\|_{\mathcal{W}}^2. \quad (16)$$

By Eq. (14), the reference differential value satisfies $\mathcal{Y}(s_t, \hat{A}_t^i) - \mathcal{Y}(s_t, \hat{A}_t^j) = \beta(d_j - d_i)$. We thus encourage the critic to preserve the same relative differences among candidate chunks:

$$\begin{aligned} \mathcal{L}_{\text{rank}}(\theta; s_t, A_t) = \mathbb{E}_{\hat{A}_t^i, \hat{A}_t^j \sim \rho(\cdot | s_t)} & \left[\ell(Q_\theta(s_t, \hat{A}_t^i) \right. \\ & \left. - Q_\theta(s_t, \hat{A}_t^j), \beta(d_j - d_i)) \right]. \end{aligned} \quad (17)$$

3.2.3 The Closed Loop of Spatio-Temporal Consistency

The interdependency of objectives. TD and EGR form a mutually reinforcing loop for safe and effective value learning. The Expected-Max TD objective provides a foundational safety layer by inherently operating within the support of the proposal distribution π_μ . However, this implicit constraint alone can still be vulnerable to selecting outlier candidates that are accidentally overestimated. EGR reinforces this safety by explicitly shaping the OOD value landscape into a geometric funnel. This structure actively biases the Best-of- N maximization toward candidates that remain close to expert behavior, providing a tighter and more reliable bound on the TD target. This enhanced safety guarantee is formalized by the following proposition:

Proposition 2 (Best-of- N bound under an EGR anchoring envelope). *Fix a demonstration pair $(s_t, A_t) \sim \mathcal{D}$ and a candidate distribution $\pi_\mu(\cdot | s_t)$. Define the EGR reference surface $\mathcal{Y}(s_t, A'_t) = \text{sg}(y_t) - \beta \|A'_t - A_t\|_{\mathcal{W}}^2$ (Eq. (14)) and the anchoring residual $\delta_\theta(s_t, A'_t) := Q_\theta(s_t, A'_t) - \mathcal{Y}(s_t, A'_t)$. Assume it is uniformly upper-bounded on the candidate set:*

$$\sup_{A'_t \in \text{supp}(\pi_\mu(\cdot | s_t))} \delta_\theta(s_t, A'_t) \leq \varepsilon.$$

Draw N candidates $\{A_t^i\}_{i=1}^N \sim \rho(\cdot | s_t)$. Then

$$\max_{i \in [N]} Q_\theta(s_t, A_t^i) \leq \text{sg}(y_t) + \varepsilon. \quad (18)$$

See Appendix B.2 for the full statement and proof.

TD Anchors and Calibrates EGR. Conversely, the TD objective provides an essential grounding signal for EGR. The TD target y_t sets the absolute scale for the EGR reference surface, preventing the geometric shaping from degenerating into an uncalibrated ranking function. This synergy allows the TD-EGR loop to progressively correct value estimates: TD provides the return-aware scale, while EGR provides the fine-grained geometric structure, jointly enabling robust ranking.

4 Experiment

In our experiments, we aim to answer the following research questions: *RQ1: Does VGAS benefit from a Transformer-based chunk critic (Q-Chunk-Former) for modeling fine-grained geometric dependencies under multimodal inputs?*

Type	Method	LIBERO-Spatial		LIBERO-Object		LIBERO-Goal		LIBERO-Long		Average	
		SR (\uparrow)	Rank (\downarrow)	SR (\uparrow)	Rank (\downarrow)	SR (\uparrow)	Rank (\downarrow)	SR (\uparrow)	Rank (\downarrow)	SR (\uparrow)	Rank (\downarrow)
BC-Only	SmolVLA	46.0	4	45.8	4	52.0	3	15.5	4	39.8	4
	QC-M	46.0	4	42.1	5	49.2	5	14.4	5	37.9	5
	QC-M+CQL	47.8	2	50.3	2	54.2	2	16.5	3	42.2	2
	QC-T+CQL	47.7	3	50.1	3	51.9	4	17.5	2	41.8	3
VGAS (Ours)		56.2	1	59.0	1	60.8	1	20.0	1	49.0	1

Table 1: Results on LIBERO (5-shot per task). SR denotes success rate (%).

RQ2: Does Explicit Geometric Regularization (EGR) improve value calibration and ranking over state-action-chunk candidates for Best-of- N selection?

4.1 Experiment Settings

Benchmark and Architecture. We evaluate **VGAS** on the widely used simulation benchmark, LIBERO [Liu *et al.*, 2023]. LIBERO is a lifelong learning benchmark focused on language-guided manipulation tasks across diverse object types, task specifications, and environments scenarios. Specifically, it includes 4 suites: Goal, Spatial, Object, and Long. Each suite is designed to evaluate a specific aspect of object manipulation and containing 10 distinct tasks. We use SmolVLA-0.5B [Shukor *et al.*, 2025] as the base chunk policy. We initialize Q-Chunk-Former with the first two decoder layers of the pre-trained SmolVLM2 [Marafioti *et al.*, 2025], keeping the critic’s token space aligned with the policy. Comprehensive architectural details are provided in Appendix D.

Baseline Method. We compare **VGAS** against a comprehensive set of baselines spanning representative paradigms for VLA fine-tuning and offline value-based improvement. **BC-only** fine-tunes SmolVLA with behavior cloning. **CQL** [Kumar *et al.*, 2020] serves as a representative conservative offline RL objective and is widely used in VLA settings [Song *et al.*, 2025; Chebotar *et al.*, 2023; Huang *et al.*, 2025]. **QC-M** follows Q-Chunking [Li *et al.*, 2025b], training an MLP critic with standard (unregularized) TD learning over action chunks. **QC-M+CQL** augments **QC-M** by adding the CQL conservative regularizer. Finally, **QC-T+CQL** retains the same objective but replaces the MLP with our Q-Chunk-Former, enabling a controlled comparison of critic architectures under identical conservative constraints. Implementation details are provided in Appendix D.2.

4.2 Main Results

Table 1 reports LIBERO success rates. The unregularized Q-Chunking baseline (**QC-M**) underperforms BC (37.9% vs. 39.8%), reflecting a maximization issue in offline RL. With sparse demonstrations, the critic can overestimate slightly off-demonstration “near-miss” chunks due to function approximation error, and Best-of- N selection then preferentially picks these overvalued outliers, inducing compounding drift under distribution shift [Kumar *et al.*, 2020].

Adding CQL alleviates this failure, improving QC-M from 37.9% to 42.2% (**QC-M+CQL**), but the gain over BC re-

mains modest. Replacing the MLP with our Transformer backbone yields a similar result (41.8% for **QC-T+CQL**), suggesting that indiscriminate conservative suppression compresses value gaps among proposal-supported candidates, leaving Best-of- N with insufficient ranking resolution.

Finally, **VGAS** achieves 49.0%, outperforming **QC-T+CQL** by a clear margin. Since both methods share the same Q-Chunk-Former backbone, this improvement is primarily attributed to Explicit Geometric Regularization (EGR). See Sec. 4.4 for further comparative analysis.

4.3 Ablation Studies

Table 2 isolates the contribution of each component. The dominant gain arises from *Explicit Geometric Regularization* (\mathcal{L}_{EGR}). Removing \mathcal{L}_{EGR} leads to a sharp drop in success rate from 49.0% to 36.4%, effectively collapsing performance back to the unregularized QC-M baseline (37.9%). This regression suggests that, without geometric shaping, the critic is susceptible to a canonical offline RL failure mode: it assigns spuriously high values to off-demo candidates, and the subsequent Best-of- N maximization amplifies these overestimations. These results indicate that EGR plays a dual role: beyond suppressing erroneous high values on off-demo actions, it explicitly structures the local value landscape around demonstrations, preserving the ranking resolution required for reliable Best-of- N selection. In addition, ablating the temporal consistency term (\mathcal{L}_{TD}) reduces performance to 45.5%, showing that while EGR provides strong spatial guidance, a TD-based anchor remains necessary to stabilize long-horizon value estimates.

Table 2: Ablation study on LIBERO (success rates (%)).

Variants	Spatial	Object	Goal	LONG	Avg
w/o SAF	51.8	54.2	56.8	17.4	45.1
w/o QCF	53.4	55	55.9	16.8	45.3
w/o \mathcal{L}_{EGR}	42.6	42.3	48.2	12.5	36.4
w/o \mathcal{L}_{TD}	55.2	54.5	56	16.4	45.5
VGAS	56.2	59.0	60.8	20.0	49

Architectural choices prove equally critical. We denote our Transformer-based critic as QCF (Q-Chunk-Former). Replacing QCF with a standard MLP backbone (w/o QCF)

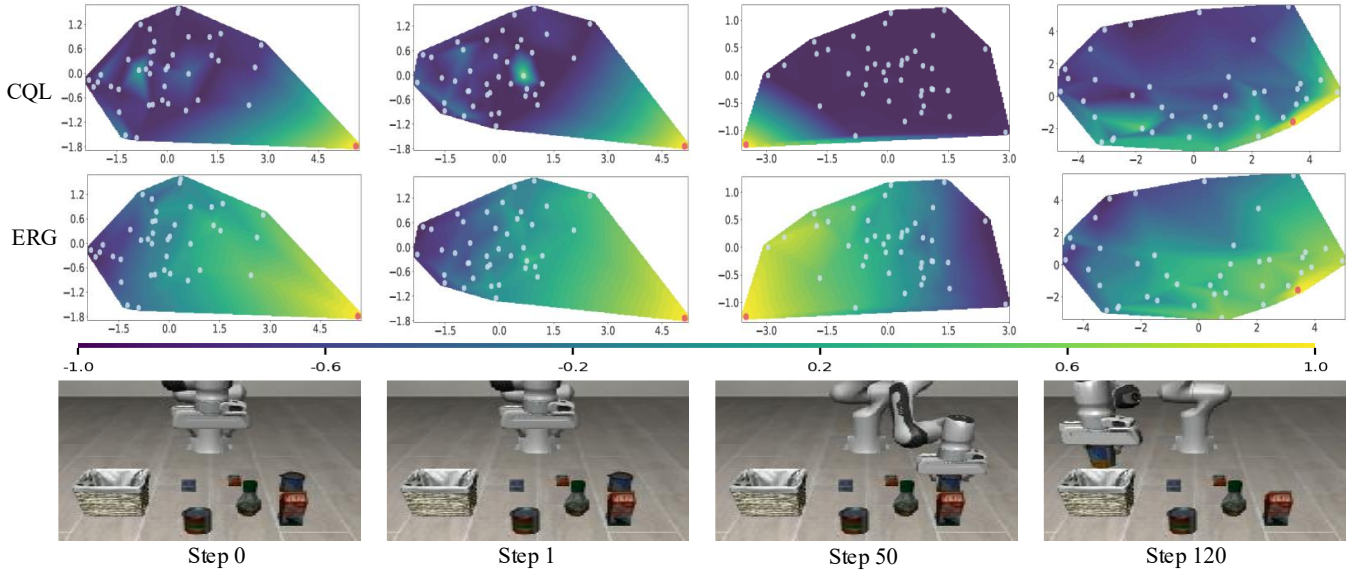


Figure 3: Visualization of the Proposal-Candidate Value Landscape: CQL vs. EGR (Ours)

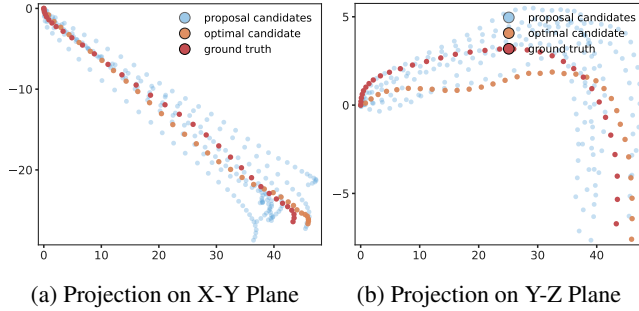


Figure 4: Multi-view Spatial Rollouts of Action Chunks and VGAS Selection. Trajectories are reconstructed via temporal integration in orthogonal views. Blue: SFT proposals; Orange: VGAS selection; Red: Ground Truth. VGAS identifies the trajectory aligning with the expert across 3D space.

yields 45.3%, validating the necessity of the Transformer’s attention mechanism for modeling complex multimodal dependencies. Notably, ablating the State-Action Fusion module (w/o SAF) further lowers performance to 45.1%. This suggests that without explicit grounding, the critic struggles to resolve fine-grained geometric ambiguities amidst high-dimensional visual features. The full framework integrates these elements to achieve the optimal success rate.

4.4 Visualization Analysis

Figure 3 visualizes the landscape of estimated action-chunk values projected onto a 2D plane, with Q -values normalized to $[-1, 1]$ for comparison. As shown in the top row, standard conservative regularization (CQL) results in a collapsed value landscape. It indiscriminately suppresses the Q -values of all proposal candidates (white dots) to a uniformly low level. Consequently, the critic loses the resolution to differentiate recoverable “near-miss” proposals from failures, rendering the selection process ineffective. In contrast, the bottom row demonstrates that VGAS successfully restores fine-grained ranking resolution. Instead of uniform suppression, the value signal exhibits a graded geometric preference that decays smoothly as candidates deviate from the expert actions (red dot). This structure ensures that the critic can meaningfully rank candidates based on their physical proximity to the optimal solution. The detailed analysis is in Appendix C.

To rigorously assess execution precision, we visualize the spatial rollouts induced by action chunks on held-out task instances. Although these instances remain semantically aligned with the training demonstrations, they contain subtle yet consequential spatial variations. The SFT baseline (blue) exhibits pronounced dispersion, producing a “cloud” of candidates that frequently drifts away from the target. This behavior is indicative of poor geometric generalization under few-shot supervision: the policy tends to memorize demonstration-specific trajectories rather than adapt its execution to instance-level spatial configurations. In contrast, VGAS acts as a geometric stabilizer. By enforcing structural consistency rather than exact path memorization, the learned critic suppresses this variance and selects the candidate (orange) that best matches the current spatial arrangement. Consequently, VGAS effectively corrects execution drift induced by rigid imitation in the base policy.

Figure 4 visualizes the multi-view spatial rollouts of action chunks and VGAS selection. Trajectories are reconstructed via temporal integration in orthogonal views. Blue: SFT proposals; Orange: VGAS selection; Red: Ground Truth. VGAS identifies the trajectory aligning with the expert across 3D space.

5 Conclusion and Limitations

In this work, we proposed VGAS, a framework that reformulates few-shot VLA adaptation from a generative modeling task to a value-guided selection problem. By decoupling high-recall semantic proposal from high-precision geometric evaluation, VGAS effectively addresses the near-miss failure modes prevalent in data-scarce regimes. We introduced the Q-Chunk-Former to resolve multimodal geometric ambiguities and proposed *Explicit Geometric Regularization* (EGR)

to prevent value landscape collapse under sparse supervision. Our experiments on the LIBERO benchmark demonstrate that VGAS significantly outperforms standard SFT and offline RL baselines, validating that explicit geometric grounding is essential for robust robotic control.

While VGAS improves success rates, the inference-time Best-of- N selection incurs higher computational latency compared to direct policy execution, potentially limiting its application in high-frequency control scenarios. Additionally, our current evaluation is confined to simulation, and extending it to real-world environments also remains a direction for future work.

Acknowledgments

The work was supported by the Australian Research Council (ARC) under Laureate project FL190100149.

References

[Bacchicocchi *et al.*, 2024] Francesco Bacchicocchi, Francesco Emanuele Stradi, Matteo Papini, Alberto Maria Metelli, Nicola Gatti, et al. Online learning with off-policy feedback in adversarial mdps. In *Proceedings of the Thirty-Third International Joint Conference on Artificial Intelligence (IJCAI-24)*, pages 3697–3705, 2024.

[Black *et al.*, 2024] Kevin Black, Noah Brown, Danny Driess, Adnan Esmail, Michael Equi, Chelsea Finn, Niccolò Fusai, Lachy Groom, Karol Hausman, Brian Ichter, et al. π_0 : A vision-language-action flow model for general robot control. *arXiv preprint arXiv:2410.24164*, 2024.

[Brohan *et al.*, 2022] Anthony Brohan, Noah Brown, Justice Carabajal, Yevgen Chebotar, Joseph Dabis, Chelsea Finn, Keerthana Gopalakrishnan, Karol Hausman, Alex Herzog, Jasmine Hsu, et al. Rt-1: Robotics transformer for real-world control at scale. *arXiv preprint arXiv:2212.06817*, 2022.

[Chebotar *et al.*, 2023] Yevgen Chebotar, Quan Vuong, Karol Hausman, Fei Xia, Yao Lu, Alex Irpan, Aviral Kumar, Tianhe Yu, Alexander Herzog, Karl Pertsch, et al. Q-transformer: Scalable offline reinforcement learning via autoregressive q-functions. In *Conference on Robot Learning*, pages 3909–3928. PMLR, 2023.

[Chen *et al.*, 2025] Yuhui Chen, Shuai Tian, Shugao Liu, Yingting Zhou, Haoran Li, and Dongbin Zhao. Conrft: A reinforced fine-tuning method for vla models via consistency policy. *arXiv preprint arXiv:2502.05450*, 2025.

[Dass *et al.*, 2022] Shivin Dass, Karl Pertsch, Hejia Zhang, Youngwoon Lee, Joseph J Lim, and Stefanos Nikolaidis. Pato: Policy assisted teleoperation for scalable robot data collection. *arXiv preprint arXiv:2212.04708*, 2022.

[Duan *et al.*, 2025] Wei Duan, Jie Lu, En Yu, and Junyu Xuan. Bandwidth-constrained variational message encoding for cooperative multi-agent reinforcement learning. *arXiv preprint arXiv:2512.11179*, 2025.

[Fu *et al.*, 2020] Justin Fu, Aviral Kumar, Ofir Nachum, George Tucker, and Sergey Levine. D4rl: Datasets for deep data-driven reinforcement learning. *arXiv preprint arXiv:2004.07219*, 2020.

[Fujimoto *et al.*, 2019] Scott Fujimoto, David Meger, and Doina Precup. Off-policy deep reinforcement learning without exploration. In *International conference on machine learning*, pages 2052–2062. PMLR, 2019.

[Ghasemipour *et al.*, 2021] Seyed Kamyar Ghasemipour, Dale Schuurmans, and Shixiang Shane Gu. Emaq: Expected-max q-learning operator for simple yet effective offline and online rl. In *International Conference on Machine Learning*, pages 3682–3691. PMLR, 2021.

[Guo *et al.*, 2025] Yanjiang Guo, Jianke Zhang, Xiaoyu Chen, Xiang Ji, Yen-Jen Wang, Yucheng Hu, and Jianyu Chen. Improving vision-language-action model with online reinforcement learning. *arXiv preprint arXiv:2501.16664*, 2025.

[Hendrycks, 2016] D Hendrycks. Gaussian error linear units (gelus). *arXiv preprint arXiv:1606.08415*, 2016.

[Huang *et al.*, 2025] Dongchi Huang, Zhirui Fang, Tianle Zhang, Yihang Li, Lin Zhao, and Chunhe Xia. Conrft: Efficient fine-tuning of vision-language-action models through chunked offline reinforcement learning. *arXiv preprint arXiv:2508.02219*, 2025.

[Intelligence *et al.*, 2025] Physical Intelligence, Kevin Black, Noah Brown, James Darpinian, Karan Dhabalia, Danny Driess, Adnan Esmail, Michael Equi, Chelsea Finn, Niccolò Fusai, et al. $\pi_{0.5}$: A vision-language-action model with open-world generalization. *arXiv preprint arXiv:2504.16054*, 2025.

[Janner *et al.*, 2022] Michael Janner, Yilun Du, Joshua B Tenenbaum, and Sergey Levine. Planning with diffusion for flexible behavior synthesis. *arXiv preprint arXiv:2205.09991*, 2022.

[Kim *et al.*, 2024] Moo Jin Kim, Karl Pertsch, Siddharth Karamchetti, Ted Xiao, Ashwin Balakrishna, Suraj Nair, Rafael Rafailov, Ethan Foster, Grace Lam, Pannag Sanketi, et al. Openvla: An open-source vision-language-action model. *arXiv preprint arXiv:2406.09246*, 2024.

[Kim *et al.*, 2025] Moo Jin Kim, Chelsea Finn, and Percy Liang. Fine-tuning vision-language-action models: Optimizing speed and success. *arXiv preprint arXiv:2502.19645*, 2025.

[Kingma, 2014] Diederik P Kingma. Adam: A method for stochastic optimization. *arXiv preprint arXiv:1412.6980*, 2014.

[Kong *et al.*, 2024] Rui Kong, Chenyang Wu, Chen-Xiao Gao, Zongzhang Zhang, and Ming Li. Efficient and stable offline-to-online reinforcement learning via continual policy revitalization. In *Proceedings of the Thirty-Third International Joint Conference on Artificial Intelligence, IJCAI-24*, pages 4317–4325, 2024.

[Kostrikov *et al.*, 2021] Ilya Kostrikov, Ashvin Nair, and Sergey Levine. Offline reinforcement learning with implicit q-learning. *arXiv preprint arXiv:2110.06169*, 2021.

[Kumar *et al.*, 2020] Aviral Kumar, Aurick Zhou, George Tucker, and Sergey Levine. Conservative Q-learning for offline reinforcement learning. In *Advances in Neural Information Processing Systems (NeurIPS)*, 2020.

[Kumar *et al.*, 2022] Aviral Kumar, Anikait Singh, Frederik Ebert, Mitsuhiro Nakamoto, Yanlai Yang, Chelsea Finn, and Sergey Levine. Pre-training for robots: Offline rl enables learning new tasks from a handful of trials. *arXiv preprint arXiv:2210.05178*, 2022.

[Levine *et al.*, 2020] Sergey Levine, Aviral Kumar, George Tucker, and Justin Fu. Offline reinforcement learning: Tutorial, review, and perspectives on open problems. *arXiv preprint arXiv:2005.01643*, 2020.

[Li *et al.*, 2025a] Haozhan Li, Yuxin Zuo, Jiale Yu, Yuhao Zhang, Zhaojun Yang, Kaiyan Zhang, Xuekai Zhu, Yuchen Zhang, Tianxing Chen, Ganqu Cui, et al. Simplevla-rl: Scaling vla training via reinforcement learning. *arXiv preprint arXiv:2509.09674*, 2025.

[Li *et al.*, 2025b] Qiyang Li, Zhiyuan Zhou, and Sergey Levine. Reinforcement learning with action chunking. *arXiv preprint arXiv:2507.07969*, 2025.

[Liu *et al.*, 2023] Bo Liu, Yifeng Zhu, Chongkai Gao, Yihao Feng, Qiang Liu, Yuke Zhu, and Peter Stone. Libero: Benchmarking knowledge transfer for lifelong robot learning. *Advances in Neural Information Processing Systems*, 36:44776–44791, 2023.

[Liu *et al.*, 2025] Jijia Liu, Feng Gao, Bingwen Wei, Xinlei Chen, Qingmin Liao, Yi Wu, Chao Yu, and Yu Wang. What can rl bring to vla generalization? an empirical study. *arXiv preprint arXiv:2505.19789*, 2025.

[Lu *et al.*, 2022] Cong Lu, Philip J Ball, Tim GJ Rudner, Jack Parker-Holder, Michael A Osborne, and Yee Whye Teh. Challenges and opportunities in offline reinforcement learning from visual observations. *arXiv preprint arXiv:2206.04779*, 2022.

[Luo *et al.*,] Kairong Luo, CAIWEI XIAO, Zhiao Huang, Zhan Ling, Yunhao Fang, and Hao Su. Dreamfuser: Value-guided diffusion policy for offline reinforcement learning.

[Lyu *et al.*, 2022] Jiafei Lyu, Xiaoteng Ma, Xiu Li, and Zongqing Lu. Mildly conservative q-learning for offline reinforcement learning. *Advances in Neural Information Processing Systems*, 35:1711–1724, 2022.

[Marafioti *et al.*, 2025] Andrés Marafioti, Orr Zohar, Miquel Farré, Merve Noyan, Elie Bakouch, Pedro Cuenca, Cyril Zakka, Loubna Ben Allal, Anton Lozhkov, Nouamane Tazi, et al. Smolvlm: Redefining small and efficient multimodal models. *arXiv preprint arXiv:2504.05299*, 2025.

[Mark *et al.*, 2024] Max Sobol Mark, Tian Gao, Georgia Gabriela Sampaio, Mohan Kumar Srirama, Archit Sharma, Chelsea Finn, and Aviral Kumar. Policy agnostic rl: Offline rl and online rl fine-tuning of any class and backbone. *arXiv preprint arXiv:2412.06685*, 2024.

[Nakamoto *et al.*, 2025] Mitsuhiro Nakamoto, Oier Mees, Aviral Kumar, and Sergey Levine. Steering your generalists: Improving robotic foundation models via value guidance. In *Conference on Robot Learning*, pages 4996–5013. PMLR, 2025.

[Sapkota *et al.*, 2025] Ranjan Sapkota, Yang Cao, Konstantinos I Roumeliotis, and Manoj Karkee. Vision-language-action models: Concepts, progress, applications and challenges. *arXiv preprint arXiv:2505.04769*, 2025.

[Schulman *et al.*, 2017] John Schulman, Filip Wolski, Prafulla Dhariwal, Alec Radford, and Oleg Klimov. Proximal policy optimization algorithms. *arXiv preprint arXiv:1707.06347*, 2017.

[Shao *et al.*, 2024] Zhihong Shao, Peiyi Wang, Qihao Zhu, Runxin Xu, Junxiao Song, Xiao Bi, Haowei Zhang, Mingchuan Zhang, YK Li, Yang Wu, et al. Deepseekmath: Pushing the limits of mathematical reasoning in open language models. *arXiv preprint arXiv:2402.03300*, 2024.

[Shin and Kim, 2023] Wonchul Shin and Yusung Kim. Guide to control: Offline hierarchical reinforcement learning using subgoal generation for long-horizon and sparse-reward tasks. In *IJCAI*, pages 4217–4225, 2023.

[Shukor *et al.*, 2025] Mustafa Shukor, Dana Aubakirova, Francesco Capuano, Pepijn Kooijmans, Steven Palma, Adil Zouitine, Michel Aractingi, Caroline Pascal, Martino Russi, Andres Marafioti, et al. Smolvla: A vision-language-action model for affordable and efficient robotics. *arXiv preprint arXiv:2506.01844*, 2025.

[Song *et al.*, 2025] Haoming Song, Delin Qu, Yuanqi Yao, Qizhi Chen, Qi Lv, Yiwen Tang, Modi Shi, Guanghui Ren, Maoqing Yao, Bin Zhao, et al. Hume: Introducing system-2 thinking in visual-language-action model. *arXiv preprint arXiv:2505.21432*, 2025.

[Sutton *et al.*, 1998] Richard S Sutton, Andrew G Barto, et al. *Reinforcement learning: An introduction*, volume 1. MIT press Cambridge, 1998.

[Sutton *et al.*, 1999] Richard S Sutton, Doina Precup, and Satinder Singh. Between mdps and semi-mdps: A framework for temporal abstraction in reinforcement learning. *Artificial intelligence*, 112(1-2):181–211, 1999.

[Tan *et al.*,] Shuhan Tan, Kairan Dou, Yue Zhao, and Philipp Krähenbühl. Interactive post-training for vision-language-action models (2025). *arXiv preprint arXiv:2505.17016*.

[Team *et al.*, 2024] Octo Model Team, Dibya Ghosh, Homer Walke, Karl Pertsch, Kevin Black, Oier Mees, Sudeep Dasari, Joey Hejna, Tobias Kreiman, Charles Xu, et al. Octo: An open-source generalist robot policy. *arXiv preprint arXiv:2405.12213*, 2024.

[Xin *et al.*, 2024] Jimmy Xin, Linus Zheng, Kia Rahmani, Jiayi Wei, Jarrett Holtz, Isil Dillig, and Joydeep Biswas. Programmatic imitation learning from unlabeled and noisy demonstrations. *IEEE Robotics and Automation Letters*, 9(6):4894–4901, 2024.

[Yu *et al.*, 2025] En Yu, Jie Lu, Xiaoyu Yang, Guangquan Zhang, and Zhen Fang. Learning robust spectral dynamics for temporal domain generalization. In *The Thirty-ninth Annual Conference on Neural Information Processing Systems*, 2025.

[Zhang and Tan, 2023] Zhe Zhang and Xiaoyang Tan. Adaptive reward shifting based on behavior proximity for offline reinforcement learning. In *IJCAI*, pages 4620–4628, 2023.

[Zhang *et al.*, 2025] Dapeng Zhang, Jing Sun, Chenghui Hu, Xiaoyan Wu, Zhenlong Yuan, Rui Zhou, Fei Shen, and Qingguo Zhou. Pure vision language action (vla) models: A comprehensive survey. *arXiv preprint arXiv:2509.19012*, 2025.

[Zhao *et al.*, 2023] Tony Z. Zhao, Vikash Kumar, Sergey Levine, and Chelsea Finn. Learning fine-grained bimanual manipulation with low-cost arms. In *Robotics: Science and Systems (RSS)*, 2023.

[Zitkovich *et al.*, 2023] Brianna Zitkovich, Tianhe Yu, Sichun Xu, Peng Xu, Ted Xiao, Fei Xia, Jialin Wu, Paul Wohlhart, Stefan Welker, Ayzaan Wahid, et al. Rt-2: Vision-language-action models transfer web knowledge to robotic control. In *Conference on Robot Learning*, pages 2165–2183. PMLR, 2023.

A Related Work

A.1 Vision-Language-Action Models.

The intersection of computer vision and robotic control has been advanced by Vision-Language-Action (VLA) models, which endow high-capacity Vision-Language Models (VLMs) with actuation capabilities to map multimodal inputs (visual observations and natural language instructions) to executable robot actions [Zitkovich *et al.*, 2023]. Representative architectures such as RT-2 [Zitkovich *et al.*, 2023], Octo [Team *et al.*, 2024], OpenVLA [Kim *et al.*, 2024], and related works [Brohan *et al.*, 2022; Black *et al.*, 2024; Intelligence *et al.*, 2025] demonstrate strong generalization across diverse tasks. A common paradigm is large-scale pre-training followed by supervised fine-tuning (SFT) on robotic demonstrations, which grounds semantic knowledge into physical control.

Despite this progress, pure imitation remains limited for efficient adaptation. SFT typically requires substantial expert coverage and can degrade sharply in few-shot regimes. Moreover, many VLAs generate actions via open-loop chunking [Zhao *et al.*, 2023], without an intrinsic mechanism to *evaluate* or *rank* candidate chunks by physical fidelity. This motivates adapting pretrained VLAs beyond static imitation by introducing explicit value-based evaluation for action-chunk selection.

A.2 Value-based Offline Reinforcement Learning.

Reinforcement learning (RL) [Levine *et al.*, 2020; Duan *et al.*, 2025] seeks policies that maximize long-horizon return [Kong *et al.*, 2024]. In the offline setting, value functions can be learned from static datasets without additional interaction, making critic-centric methods attractive when online rollouts [Bacchicocchi *et al.*, 2024] are costly or unsafe. To prevent extrapolation errors, Conservative offline RL methods [Kumar *et al.*, 2020] mitigate extrapolation error by suppressing values of out-of-distribution (OOD) actions [Zhang and Tan, 2023], while implicit approaches like IQL [Kostrikov *et al.*, 2021] tend to avoid OOD actions via behavior-regularized policy extraction.

Sampling-based Maximization (Best-of- N). In continuous action spaces, directly computing $\max_a Q(s, a)$ is often intractable. A widely used surrogate is *proposal-constrained maximization*: sample N candidate actions from a behavior-aligned proposal (or a learned generative model) and select the argmax under a critic. BCQ [Fujimoto *et al.*, 2019] is a canonical example, using a state-conditioned generative model to produce in-distribution candidates and choosing the highest-valued action via a learned Q-function. EMaQ [Ghasemipour *et al.*, 2021] formalizes this principle via an *Expected-Max* backup operator that interpolates between evaluation and maximization through the number of samples N , providing an operator-level view of Best-of- N style policy improvement. More recently, generative planners such as Diffuser [Janner *et al.*, 2022] and value-guided diffusion methods [Luo *et al.*,] similarly combine sampling with value-based guidance or reranking over action sequences or trajectories, sharing the core idea of improving decision quality through learned value signals.

A.3 RL for VLA Models.

Integrating RL into VLA models aims to combine semantic reasoning with return-driven optimization. A core challenge is that modern VLAs often execute *action chunks* (temporally extended sequences) rather than atomic actions, which shifts both credit assignment and value estimation from the single-step regime to the chunk level. Moreover, unlike traditional RL that operates on compact state vectors, VLAs condition on high-dimensional multimodal inputs (vision, language, and proprioception), making stable value learning sensitive to cross-modal fusion and representation balance.

Action Chunk Value learning. Recent works extend value learning to action chunking by treating a short-horizon action sequence as a single decision unit [Li *et al.*, 2025b], showing that chunk-level Q-functions can improve temporal consistency. This line of work also introduces unbiased n -step backup targets to stabilize and accelerate TD learning under temporally extended actions. While promising in low-dimensional state settings, scaling chunk-level critics to high-dimensional multimodal inputs (vision, language, and proprioception) remains challenging.

Online Fine-tuning. A line of work fine-tunes VLAs via online RL or interactive learning [Li *et al.*, 2025a; Tan *et al.*, ; Mark *et al.*, 2024; Guo *et al.*, 2025]. These methods typically do not learn an explicit Q-function; instead, they update the policy using on-policy algorithms such as PPO [Schulman *et al.*, 2017] or GRPO [Shao *et al.*, 2024], where policy gradients are estimated from trajectory-level advantage signals. While effective, online fine-tuning can incur substantial interaction costs and safety concerns, making it less practical for rapid few-shot adaptation. Moreover, trajectory-level supervision can provide relatively coarse credit assignment, which may be insufficient to correct fine-grained geometric errors in long-horizon manipulation.

Offline Value Learning. Alternatively, approaches such as Q-Transformer [Chebotar *et al.*, 2023] learn Q-functions from offline data to enable end-to-end control. More closely related to our setting, V-GPS [Nakamoto *et al.*, 2025] and Hume [Song *et al.*, 2025] also learn value functions from offline datasets and make decisions by scoring and selecting among candidate actions. Similarly, ConRFT [Chen *et al.*, 2025] improves VLA policies via offline RL. However, most of these methods are primarily formulated for single-step action evaluation and thus do not directly align with chunk-based VLA policies that execute temporally-extended action sequences. Moreover, these approaches [Chebotar *et al.*, 2023; Nakamoto *et al.*, 2025; Song *et al.*, 2025] typically compress multimodal observations into a single latent vector for value prediction, which can discard fine-grained cues needed for accurate value estimation and precise action ranking.

B Theoretical Analysis

In this appendix, we provide proofs for the convergence properties of the *Proposal-Constrained Chunked Expected-Max* operator introduced in Sec. 3.2. Our analysis adapts the operator-level argument of EMaQ [Ghasemipour *et al.*, 2021] to the induced semi-Markov decision process (SMDP) formed by length- h action chunks.

B.1 Convergence of the Chunked Expected-Max Operator

Induced SMDP and bounded function space. Let $A = (a_0, \dots, a_{h-1}) \in \mathcal{A}^h$ denote an action chunk. We consider the induced SMDP with (i) the chunked discounted return

$$R_h(s, A) := \mathbb{E} \left[\sum_{k=0}^{h-1} \gamma^k r(s_k, a_k) \mid s_0 = s, A \right], \quad (19)$$

(ii) the h -step transition kernel $\mathcal{P}^h(\cdot \mid s, A)$, and (iii) the effective discount factor γ^h . Assume bounded one-step rewards $|r(s, a)| \leq r_{\max}$ and $\gamma \in (0, 1)$. Then

$$|R_h(s, A)| \leq \sum_{k=0}^{h-1} \gamma^k r_{\max} = \frac{r_{\max}(1 - \gamma^h)}{1 - \gamma} =: R_{\max}. \quad (20)$$

Let \mathcal{B} denote the space of bounded real-valued functions over chunk state-action pairs:

$$\mathcal{B} := \{Q : \mathcal{S} \times \mathcal{A}^h \rightarrow \mathbb{R} \mid \|Q\|_{\infty} < \infty\}, \quad \|Q\|_{\infty} := \sup_{(s, A)} |Q(s, A)|.$$

(We assume Q is bounded and measurable; the analysis extends to continuous \mathcal{A}^h (equivalently $\mathcal{B} = L_{\infty}(\mathcal{S} \times \mathcal{A}^h)$ under $\|\cdot\|_{\infty}$).

Definition 1 (Chunked Expected-Max Operator). *Fix a proposal distribution $\pi_{\mu}(A \mid s)$ over action chunks and an integer $N \geq 1$. Define $\mathcal{T}_{\mu}^N : \mathcal{B} \rightarrow \mathcal{B}$ by*

$$(\mathcal{T}_{\mu}^N Q)(s, A) := R_h(s, A) + \gamma^h \mathbb{E}_{s' \sim \mathcal{P}^h(\cdot \mid s, A)} \left[\mathbb{E}_{A'_{1:N} \sim \pi_{\mu}(\cdot \mid s')} \left[\max_{i \in [N]} Q(s', A'_i) \right] \right]. \quad (21)$$

Lemma 1 (Well-definedness). *Assume $|r(s, a)| \leq r_{\max}$ and $\gamma \in (0, 1)$, hence $|R_h(s, A)| \leq R_{\max}$ as in (20). Then for any $Q \in \mathcal{B}$,*

$$\|\mathcal{T}_{\mu}^N Q\|_{\infty} \leq R_{\max} + \gamma^h \|Q\|_{\infty}.$$

In particular, $\mathcal{T}_{\mu}^N Q \in \mathcal{B}$.

Proof. For any $Q \in \mathcal{B}$ and (s, A) , let $s' \sim \mathcal{P}^h(\cdot \mid s, A)$. We have:

$$|(\mathcal{T}_{\mu}^N Q)(s, A)| \leq |R_h(s, A)| + \gamma^h \mathbb{E}_{s' \sim \mathcal{P}^h(\cdot \mid s, A)} \left[\max_{i \in [N]} |Q(s', A'_i)| \right] \leq R_{\max} + \gamma^h \|Q\|_{\infty},$$

since $\max_i |Q(s', A'_i)| \leq \|Q\|_{\infty}$. Taking $\sup_{(s, A)}$ yields the claim. \square

Lemma 2 (Non-expansiveness of expected max). *Let u, v be bounded functions and let X_1, \dots, X_N be random variables. Then*

$$\left| \mathbb{E} \left[\max_{i \in [N]} u(X_i) \right] - \mathbb{E} \left[\max_{i \in [N]} v(X_i) \right] \right| \leq \|u - v\|_{\infty}. \quad (22)$$

Proof. Using $|\mathbb{E}[Z]| \leq \mathbb{E}[|Z|]$,

$$\left| \mathbb{E} \left[\max_i u(X_i) - \max_i v(X_i) \right] \right| \leq \mathbb{E} \left[\left| \max_i u(X_i) - \max_i v(X_i) \right| \right].$$

For any realizations $\{x_i\}$,

$$\left| \max_i u(x_i) - \max_i v(x_i) \right| \leq \max_i |u(x_i) - v(x_i)| \leq \|u - v\|_{\infty}.$$

Taking expectation completes the proof. \square

Theorem 1 (γ^h -Contraction). *For any $N \geq 1$, the operator \mathcal{T}_{μ}^N is a γ^h -contraction under $\|\cdot\|_{\infty}$:*

$$\|\mathcal{T}_{\mu}^N Q_1 - \mathcal{T}_{\mu}^N Q_2\|_{\infty} \leq \gamma^h \|Q_1 - Q_2\|_{\infty}, \quad \forall Q_1, Q_2 \in \mathcal{B}.$$

Consequently, \mathcal{T}_{μ}^N admits a unique fixed point $Q_{\mu}^N \in \mathcal{B}$ and $(\mathcal{T}_{\mu}^N)^k Q_0 \rightarrow Q_{\mu}^N$ for any $Q_0 \in \mathcal{B}$.

Proof. Fix (s, A) and let $Q_1, Q_2 \in \mathcal{B}$. The reward terms cancel:

$$\begin{aligned} |(\mathcal{T}_\mu^N Q_1)(s, A) - (\mathcal{T}_\mu^N Q_2)(s, A)| &= \gamma^h \left| \mathbb{E}_{s'} \left[g_N(Q_1)(s') - g_N(Q_2)(s') \right] \right| \\ &\leq \gamma^h \mathbb{E}_{s'} \left| g_N(Q_1)(s') - g_N(Q_2)(s') \right|, \end{aligned}$$

where

$$g_N(Q)(s') := \mathbb{E}_{A'_{1:N} \sim \pi_\mu(\cdot | s')} \left[\max_{i \in [N]} Q(s', A'_i) \right].$$

Applying Lemma 2 to $u(\cdot) = Q_1(s', \cdot)$ and $v(\cdot) = Q_2(s', \cdot)$ yields $|g_N(Q_1)(s') - g_N(Q_2)(s')| \leq \|Q_1 - Q_2\|_\infty$ for all s' . Thus

$$|(\mathcal{T}_\mu^N Q_1)(s, A) - (\mathcal{T}_\mu^N Q_2)(s, A)| \leq \gamma^h \|Q_1 - Q_2\|_\infty.$$

Taking $\sup_{(s, A)}$ gives the contraction inequality. Since $\gamma^h < 1$ and Lemma 1 ensures $\mathcal{T}_\mu^N : \mathcal{B} \rightarrow \mathcal{B}$, Banach's fixed-point theorem implies existence/uniqueness and convergence. \square

Proposition 3 (Monotonicity in N). *Let Q_μ^N denote the unique fixed point of \mathcal{T}_μ^N . For any integers $N > M \geq 1$, we have*

$$Q_\mu^N(s, A) \geq Q_\mu^M(s, A), \quad \forall s \in \mathcal{S}, \forall A \in \text{supp}(\pi_\mu(\cdot | s)).$$

Proof. For any bounded Q and any (s, A) , draw $A'_{1:N} \sim \pi_\mu(\cdot | s')$ once and use the first M samples for the M -sample backup. Then for every realization,

$$\max_{i \in [N]} Q(s', A'_i) \geq \max_{i \in [M]} Q(s', A'_i).$$

Taking expectation over $A'_{1:N}$ and s' yields $(\mathcal{T}_\mu^N Q)(s, A) \geq (\mathcal{T}_\mu^M Q)(s, A)$. Now apply the above pointwise inequality to Q_μ^M . Since $Q_\mu^M = \mathcal{T}_\mu^M Q_\mu^M$, we have $Q_\mu^M \leq \mathcal{T}_\mu^N Q_\mu^M$. Moreover, \mathcal{T}_μ^N is order-preserving in Q (max and expectation preserve order), hence $(\mathcal{T}_\mu^N)^k Q_\mu^M \geq Q_\mu^M$ for all k . Taking $k \rightarrow \infty$ and using Theorem 1 yields $Q_\mu^N = \lim_{k \rightarrow \infty} (\mathcal{T}_\mu^N)^k Q_\mu^M \geq Q_\mu^M$. \square

Theorem 2 (Limit as $N \rightarrow \infty$ (sketch)). *Under standard regularity assumptions (e.g., no ties / continuous proposal density), the fixed points $\{Q_\mu^N\}_{N \geq 1}$ converge pointwise to the optimal value function whose actions are restricted to the support of π_μ , denoted $Q_{\pi_\mu}^*$:*

$$\lim_{N \rightarrow \infty} Q_\mu^N = Q_{\pi_\mu}^*.$$

Proof sketch. For any fixed Q and state s' , define

$$g_N(Q)(s') = \mathbb{E}_{A'_{1:N} \sim \pi_\mu(\cdot | s')} \left[\max_{i \in [N]} Q(s', A'_i) \right].$$

Then $g_N(Q)(s')$ is non-decreasing in N and converges to the essential supremum of $Q(s', A)$ over $A \sim \pi_\mu(\cdot | s')$. Consequently, \mathcal{T}_μ^N converges (pointwise) to the support-restricted optimality operator. Monotonicity in N (Prop. 3), together with contraction (Thm. 1), yields convergence of the fixed points; see the corresponding EMaQ analysis [Ghasemipour *et al.*, 2021]. \square

B.2 EGR Anchoring Envelope and Best-of- N Bound

We formalize how the EGR regression objective induces an *upper-envelope* inequality over off-demo candidates sampled from $\rho(\cdot | s_t)$, and how such an envelope immediately bounds the Best-of- N maximization used in the chunked TD target.

Setup. Fix a data (demonstration) pair $(s_t, A_t) \sim \mathcal{D}$ and an auxiliary candidate distribution $\rho(\cdot | s_t)$. Recall the EGR reference surface (Eq. (14)):

$$\mathcal{Y}(s_t, A'_t) := \text{sg}(y_t) - \beta \|A'_t - A_t\|_{\mathcal{W}}^2, \quad (23)$$

where $\beta > 0$ and y_t is the chunk-level TD anchor (Eq. (12)). Define the pointwise EGR residual

$$\delta_\theta(s_t, A'_t) := Q_\theta(s_t, A'_t) - \mathcal{Y}(s_t, A'_t). \quad (24)$$

From EGR regression to an upper envelope. The anchoring loss encourages $\delta_\theta(s_t, A'_t)$ to be small on candidates $A'_t \sim \rho(\cdot | s_t)$. To make this statement explicit, we assume the residual is uniformly upper-bounded on the candidate set.

Lemma 3 (Anchoring-induced upper envelope via a residual bound). *Assume the residual admits a uniform upper bound on the candidate set:*

$$\sup_{A'_t \in \text{supp}(\rho(\cdot | s_t))} \delta_\theta(s_t, A'_t) \leq \varepsilon, \quad (25)$$

for some $\varepsilon \geq 0$. Then for all $A'_t \in \text{supp}(\rho(\cdot | s_t))$ we have the upper-envelope inequality

$$Q_\theta(s_t, A'_t) \leq \text{sg}(y_t) - \beta \|A'_t - A_t\|_{\mathcal{W}}^2 + \varepsilon. \quad (26)$$

Proof. From the residual definition in (24), for any A'_t we have the identity

$$Q_\theta(s_t, A'_t) = \mathcal{Y}(s_t, A'_t) + \delta_\theta(s_t, A'_t). \quad (27)$$

For any $A'_t \in \text{supp}(\rho(\cdot | s_t))$, the bound Eq. (25) implies $\delta_\theta(s_t, A'_t) \leq \varepsilon$. Substituting into Eq. (27) yields $Q_\theta(s_t, A'_t) \leq \mathcal{Y}(s_t, A'_t) + \varepsilon$. Finally, plugging in Eq. (23) gives Eq. (26). \square

Bounding Best-of- N under the envelope. We now show the envelope immediately bounds the Best-of- N maximization. Recall that the EGR loss is minimized over a broad OOD distribution $\rho(\cdot | s_t)$. In our implementation (Appendix D), ρ is constructed as a mixture that explicitly includes samples from the proposal policy π_μ . Consequently, $\text{supp}(\pi_\mu) \subseteq \text{supp}(\rho)$. Thus, if the envelope holds for ρ , it naturally holds for π_μ .

Proposition 4 (Best-of- N bound under an EGR-style upper envelope). *Let $(s_t, A_t) \sim \mathcal{D}$ and let $\pi_\mu(\cdot | s_t)$ be the candidate sampling distribution. Draw N candidates $\{A'^i_t\}_{i=1}^N \sim \pi_\mu(\cdot | s_t)$. If the envelope Eq. (26) holds for all $A'_t \in \text{supp}(\pi_\mu(\cdot | s_t))$ (inherited from ρ), then*

$$\max_{i \in [N]} Q_\theta(s_t, A'^i_t) \leq \text{sg}(y_t) - \beta \min_{i \in [N]} \|A'^i_t - A_t\|_{\mathcal{W}}^2 + \varepsilon \leq \text{sg}(y_t) + \varepsilon. \quad (28)$$

Proof. Apply Eq. (26) to each sampled candidate A'^i_t :

$$Q_\theta(s_t, A'^i_t) \leq \text{sg}(y_t) - \beta \|A'^i_t - A_t\|_{\mathcal{W}}^2 + \varepsilon.$$

Taking $\max_{i \in [N]}$ on both sides gives

$$\max_{i \in [N]} Q_\theta(s_t, A'^i_t) \leq \max_{i \in [N]} (\text{sg}(y_t) - \beta \|A'^i_t - A_t\|_{\mathcal{W}}^2 + \varepsilon).$$

Since $\text{sg}(y_t)$ and ε do not depend on i , and $-\beta(\cdot)$ is decreasing in the distance term,

$$\max_{i \in [N]} (\text{sg}(y_t) - \beta \|A'^i_t - A_t\|_{\mathcal{W}}^2 + \varepsilon) = \text{sg}(y_t) - \beta \min_{i \in [N]} \|A'^i_t - A_t\|_{\mathcal{W}}^2 + \varepsilon,$$

which proves the first inequality in Eq. (28). The second inequality follows since $\min_i \|A'^i_t - A_t\|_{\mathcal{W}}^2 \geq 0$. \square

Remark. The residual bound Eq. (25) is not an additional algorithmic constraint: it is a compact way to express that the EGR regression error on the candidate set is small. In practice, ε can be interpreted as the worst-case anchoring fit error over candidates drawn from $\pi_\mu(\cdot | s_t)$.

C Visualization Methodology and Detailed Analysis

Figure 3 visualizes the landscape of estimated state-action-chunk values on the LIBERO-Object benchmark. To interpret the high-dimensional action chunks (dimension $h \times d_{\text{action}}$), we use Principal Component Analysis (PCA) to project proposal candidates and ground-truth (GT) demonstrations onto a 2D plane, normalizing estimated Q -values to $[-1, 1]$ for comparison. The color gradient—from yellow (high value) to dark blue (low value)—reveals a stark contrast in landscape topology between the two approaches. The top row shows that CQL-style regularization results in a collapsed value landscape: it indiscriminately suppresses all proposal candidates (white dots) to a uniformly low value regardless of their quality, failing to differentiate “near-miss” proposals from failures. In contrast, the bottom row demonstrates that VGAS (with EGR) discriminative value landscape. Instead of a binary plateau, the value signal exhibits a graded geometric preference, decaying smoothly as candidates deviate from the expert trajectory. This confirms that EGR acts as a structural inductive bias, enabling the critic to meaningfully rank candidates based on their physical proximity to the optimal solution.

We further observe distinct spatial and temporal characteristics in the learned landscapes. Spatially, there is a visible gap between the proposal distribution and the GT (red dot); we attribute this to the mean-seeking bias of the SFT policy, which tends to generate smoothed trajectories compared to the sharper, high-frequency control signals of human experts. Crucially, VGAS maintains a valid gradient across this gap, guiding selection toward the expert mode despite the distribution shift. Temporally, the value maps exhibit dynamic coherence: adjacent timesteps ($t = 0$ and $t = 1$) share similar topologies, whereas distant steps ($t = 50$ and $t = 120$) show significant structural differences. This indicates that the VGAS does not merely memorize static geometric relations but adaptively adjusts its estimation according to evolving real-world dynamics, providing state-aware guidance throughout the entire task horizon.

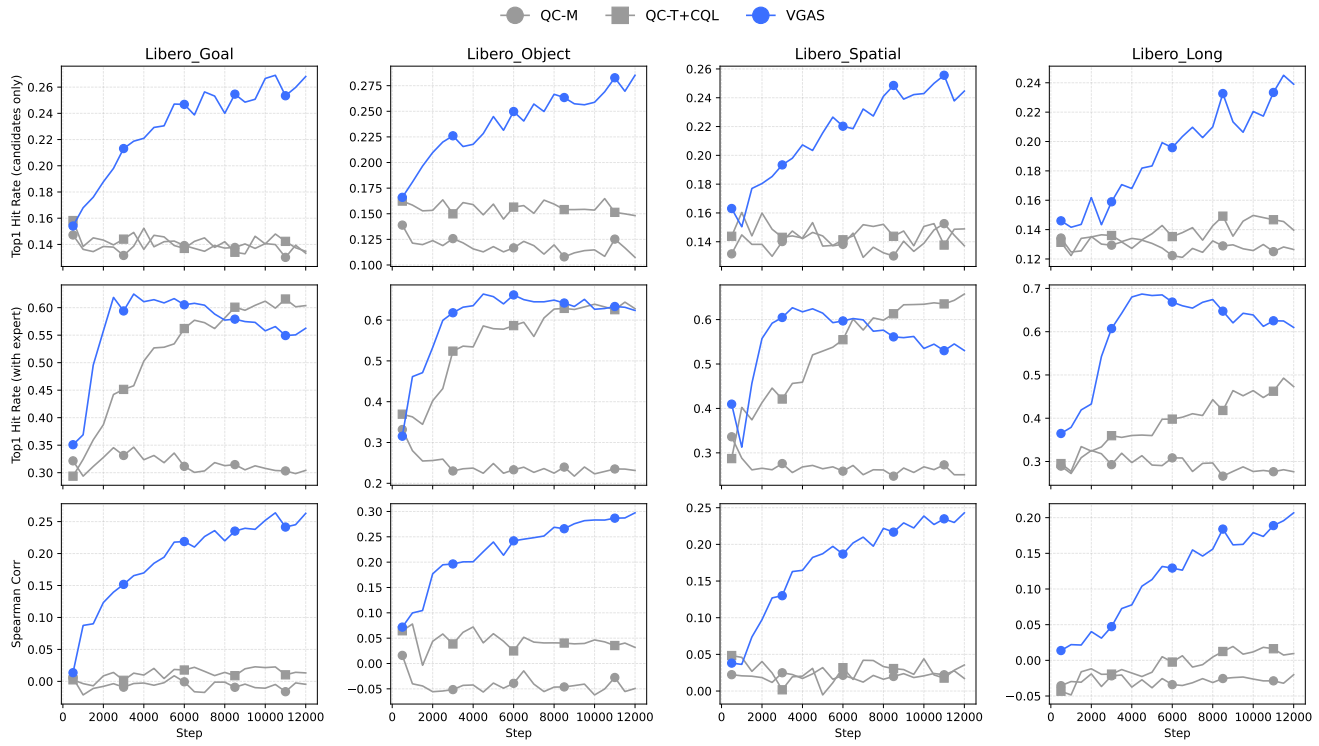


Figure 5: Offline Ranking Evaluation on Held-out Data.

D Implementation Details

D.1 Experimental Setup

(i) Reward function. Consistent with real-world scenarios where explicit rewards are scarce, the LIBERO dataset contains no reward annotations. We therefore construct a sparse binary reward by labeling the last h steps of each demonstration rollout as successful. Following [Nakamoto *et al.*, 2025], we set $h = 3$. Additionally, we use shifted rewards $\{-1, 1\}$ instead of $\{0, 1\}$, which we found to yield more stable learning in practice.

(ii) Training protocol. We first perform supervised fine-tuning (SFT) of the VLA model using 5-shot expert demonstrations per task, randomly sampled from the LIBERO dataset. We then train a critic using different variants of offline RL (ORL) objectives on the resulting offline data.

(iii) OOD candidate generation. Following the conservative offline RL intuition (e.g., CQL) that penalizes actions with low support under the offline dataset, we construct OOD candidates by sampling from $\rho(\cdot | s_t)$, instantiated as a mixture of: (i) proposals from the frozen VLA policy $\pi_\mu(\cdot | s_t)$; (ii) Gaussian perturbations of the demonstration (ground-truth) chunk A_t (GT+noise); (iii) prefix-truncated variants of A_t (early-terminated chunks); and (iv) linear interpolations between the demonstration chunk and a policy proposal, i.e., $\tilde{A}_t = \alpha A_t + (1 - \alpha) \hat{A}_t$. and $\alpha \in [0, 1]$.

(iv) Backbone Architecture Details. We adopt SmolVLA-0.5B [Shukor *et al.*, 2025] as the underlying policy backbone. Built upon the SmolVLM2 architecture, it employs a SigLIP visual encoder to process high-dimensional observations. These visual tokens are fused with language instructions and proprioceptive states within a decoder-only Transformer. The policy head utilizes a flow-matching objective to generate high-dimensional action chunks in parallel, which serves as the proposal distribution for our VGAS framework.

D.2 Baseline Implementation Details

Base Policy Training. To evaluate performance in a realistic data-scarce regime, we adopt a standardized two-stage training protocol for all methods. First, we obtain the base proposal policy π_μ by fine-tuning the SmolVLA backbone using only 5 expert demonstrations per task, randomly sampled from the LIBERO benchmark². This fine-tuning is conducted via the official LeRobot repository³. In the second stage, we freeze this few-shot adapted policy to serve as a static proposal generator.

²<https://huggingface.co/datasets/HuggingFaceVLA/libero>

³<https://github.com/huggingface/lerobot>

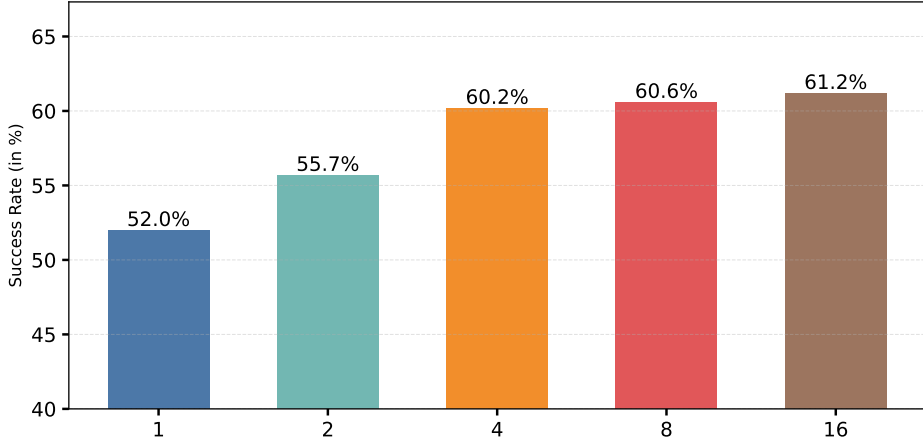


Figure 6: Impact of Inference Budget N . Evaluation on LIBERO-Goal showing monotonic improvement from the baseline ($N = 1$) to saturation around $N = 8$.

Crucially, the offline dataset \mathcal{D} used to train the critic (for both VGAS and baselines) is constructed exclusively from these same 5-shot demonstrations, ensuring that value learning operates under the same strict data-scarce constraints.

Baseline Configurations. Unless stated otherwise, all methods keep π_μ fixed and differ only in the critic objective and architecture.

- **BC-Only:** This baseline directly executes the base policy π_μ obtained in the first stage without any test-time selection.
- **QC-M (Q-Chunking-MLP):** Q-Chunking [Li *et al.*, 2025b] proposes two variants: QC (Best-of- N backup) and QC-FQL (Flow Matching distillation). We adopt the QC variant for direct comparison. Following the official implementation, we use an MLP critic with hidden dimensions [512, 512, 512, 512]. For state encoding, we pool the VLM tokens (I_t, L_t and p_t) from the backbone into a fixed representation (dim=960). The action chunk ($h \times d_a$) is flattened and projected via an MLP to match the state dimension. Finally, the state and action chunk representations are concatenated and fed into the critic.
- **QC-M+CQL:** We augment QC-M by adding the CQL regularization term. We use the default coefficient $\alpha = 5.0$, which performs comparably to alternative choices (e.g., $\alpha = 2.0$) in our validation. The negative (OOD) action pool is sampled from the proposal-centered distribution $\pi_\mu(\cdot | s_t)$, ensuring alignment with our method’s $\rho(\cdot | s_t)$ construction for fair comparison
- **QC-T+CQL:** We retain the QC-M+CQL objective but replace the MLP backbone with our Transformer-based Q-Chunk-Former. This baseline isolates the effect of critic architecture under identical conservative constraints.

Shared rollout settings. Unless otherwise specified, all methods use the same chunk length $h = 32$ (or $h = 50$ for LIBERO-Long) to estimate $Q(s_t, A_t)$, where $A_t := (a_t, a_{t+1}, \dots, a_{t+h-1})$ denotes an h -step action chunk. During execution, we apply only the first $n_{\text{exec}} = 20$ action steps of each selected chunk, i.e., $(a_t, a_{t+1}, \dots, a_{t+n_{\text{exec}}-1})$ with $n_{\text{exec}} < h$.

VGAS. We report the complete list of hyperparameters in Table 3, and task-specific overrides in Table 4. Our Q-Chunk-Former is initialized from the first two layers of the SmolVLM backbone. We directly reuse the multimodal features extracted by the frozen SmolVLM (i.e., the output of the SmolVLA encoder) as the vision–language input to Q-Chunk-Former. In our notation, the *Q-chunk length h* denotes the length of an action chunk, while *N-action-step* indicates that we execute only the first N primitive actions within each predicted chunk at rollout. We use clipped double Q-learning: the TD target is computed using the minimum of the two target critics.

D.3 Weighted metric implementation Details

In the Explicit Geometric Regularization (EGR) objective (Eq. 14 and Eq. 17), the term $\|\hat{A}_t - A_t\|_{\mathcal{W}}^2$ denotes a *weighted squared Euclidean distance*, averaged over the valid horizon of an action chunk. This metric prioritizes critical action dimensions (e.g., end-effector translation) and supports variable-length chunks via a padding mask.

Let $A \in \mathbb{R}^{h \times d_a}$ be the ground-truth action chunk and $\hat{A} \in \mathbb{R}^{h \times d_a}$ be a candidate chunk, where h is the chunk size and d_a is the action dimension (for LIBERO, typically $d_a = 7$: 3D end-effector position, 3D end-effector orientation (a 3-parameter representation), and 1D gripper control). Let $w \in \mathbb{R}^{d_a}$ be a nonnegative weight vector. We define the masked, weighted

Table 3: Hyperparameters for VGAS.

Hyperparameter	Value
Learning rate	0.0001
Optimizer	Adam [Kingma, 2014]
Warm up step	1000
Gradient steps	12000 (default), 20000 (Libero-Goal, Libero-long)
Gradient-clip	10.0
Minibatch size	32
Q-chunk-Former layers	2
Q-chunk-Former hidden dimensions	960
State-Action-Fusion Mlp dimensions	960
Q chunk len	32(default), 50 (Libero Long)
N-action-step	20
Vlaue Head MLP dimensions	[512, 512]
Vlaue head Nonlinearity	GELU [Hendrycks, 2016]
Target network smoothing coefficient	0.005
Discount factor γ	0.98 (default), 0.99 (Libero-Long)
Clipped double Q-learning	True
Q aggregation (twin critics)	Min

Table 4: Hyperparameters for Different Task suit.

Task suit	λ	β	η	w
Libero-Spatial	5.0	5.0	1.0	5 5 5 1 1 1 1
Libero-Goal	5.0	5.0	1.0	5 5 5 1 1 1 1
Libero-Object	2.0	2.0	1.0	5 5 5 1 1 1 1
Libero-Long	5.0	5.0	1.0	5 5 5 1 1 1 1

squared distance as

$$\|\hat{A} - A\|_{\mathcal{W}}^2 = \frac{1}{\sum_{k=1}^H m_k} \sum_{k=1}^H m_k \sum_{j=1}^{d_a} w_j (\hat{a}_{k,j} - a_{k,j})^2, \quad (29)$$

where:

- $m_k \in \{0, 1\}$ is a binary mask indicating whether time step k is valid (i.e., non-padding),
- $\hat{a}_{k,j}$ and $a_{k,j}$ denote the j -th action dimension at step k for \hat{A} and A , respectively,
- $w = [w_1, \dots, w_{d_a}]$ specifies the relative importance of each control dimension.

Weight configuration. As shown in Table 4, we set $w = [5, 5, 5, 1, 1, 1, 1]$, assigning weight 5.0 to translational components (x, y, z) and weight 1.0 to rotation and gripper states. Empirically, penalizing position errors more heavily encourages the critic to emphasize trajectory precision, which is crucial for manipulation success.

E Additional Experimental Results and Analysis

E.1 Training Dynamics and Critic Ranking Resolution

To verify the critic’s generalization ability, we evaluate it offline on a held-out set of 45 unseen expert episodes per task. For each observation, we sample $N = 8$ proposal candidates and report the Top-1 Hit Rate (the probability of selecting the proposal that is geometrically closest to the expert) and the Spearman correlation. Fig. 5 reveals three key findings. First, VGAS consistently assigns higher scores to candidates that remain close to the expert, which reduces overestimation on geometrically divergent OOD actions and supports safer selection on unseen states where the policy may drift. Second, the high hit rate indicates that VGAS builds a discriminative value landscape within the proposal set. In contrast, CQL tends to flatten local value differences, weakening ranking resolution. VGAS preserves a clear ordering among “near-miss” candidates, making superior candidates easier to separate from inferior ones. Finally, comparing the “With Expert” setting (middle row) and the “Candidates Only” setting (top row) highlights an important difference. CQL can assign high scores to the exact expert action when it is present, but it is less reliable at selecting the most expert-like candidate when the ground truth is absent. VGAS performs well in both settings. Although geometric proximity is not a perfect proxy for task success, it provides a practical signal in the few-shot imitation regime, where unconstrained maximization is brittle.

E.2 Sensitivity to Inference Budget

We study how the number of sampled proposals N affects VGAS, using the LIBERO-Goal suite as a representative case. As shown in Fig. 6, the success rate increases monotonically with the inference budget. Starting from the base policy ($N=1$, 52.0%), applying Best-of- N selection yields substantial gains, reaching 60.2% with only $N=4$. This rapid improvement indicates that the proposal policy often generates high-quality “near-miss” candidates that are not selected under greedy sampling but can be reliably retrieved by our geometrically regularized critic. Beyond $N=8$ (60.6%), the gains diminish, with only a marginal improvement at $N=16$ (61.2%). We therefore use $N=8$ as the default, balancing performance against inference latency in the main experiments.